ADVANCED FUNCTIONAL MATERIALS
www.afm-journal.de

A Green and Effective Organocatalyst for Faster Oxidation of Li_2S in Electrochemical Processes

Qining Fan, Shilin Zhang, Jicheng Jiang, Wilford Lie, Wei Kong Pang, Qinfen Gu, Weishen Yang, Huakun Liu, Jiazhao Wang, and Zaiping Guo**

The search for viable carbon-neutral sources of renewable energy is one of the most critical challenges in science today. The chemical community is committed to seeking efficient, inexpensive, and sustainable electrocatalysts that can exploit the energy produced by sustainable energy resources. Here, an ethanol organocatalyst, which is green and cheap, that can efficiently catalyze the oxidation of Li_2S in the electrochemical reactions of Li_2S cathodes is identified . This study demonstrates that a multitude of small molecular organocatalysts will offer electrochemists an elegant tool for accelerating electrochemical reactions with otherwise unattainable efficiency and precision. This concept refashions electrochemical domains and has broad implications for the design of "green" and sustainable chemistry cycles.

1. Introduction

The development of completely carbon-neutral industrialization requires reducing society's reliance on fossil fuels by increasing the use of sustainable fuels and identifying chemical building blocks from renewable sources. Electrocatalysis-based devices, such as water electrolyzers, fuel cells, and metal–air/sulfurbatteries, allow the conversion between chemical energy and electricity that can be used in future systems for the storage and use of renewable energy.[1] One of the most attractive choices of electrocatalyst for these processes involves solid materials (such as metals and carbons), consisting of well-defined structures and surfaces that provide abundant active sites on which chemical reactions are accelerated.[2] So far, based on a profound understanding of the fundamental principles of such electrocatalysts, significant improvements have been achieved in the design of electrocatalysts with characteristic reactivity, durability, and selectivity, in order to meet special electrocatalysis process needs.[3] Nevertheless, the problem of handling toxic agents and solvents, complicated catalyst design, the generation of hazardous derivatives, and/or the consumption of scarce sources during conventional catalyst preparation, are restricting them from new and widespread applications. Serious research endeavors are thus required to focus on reconfiguring the electrocatalysts to efficiently accelerate electrochemical reactions in a greener manner than traditional catalysts, as this remains a significant challenge for the fundamental science.

Organocatalysis, or the use of small organic molecules for the synthesis of natural products, is well recognized as a critical part of the catalytic toolbox for asymmetric catalysis because, compared with conventional catalysts (i.e., Platinum, Nickel, Carbon, etc.), they are simpler to design and modify, commercially available and/or easily synthesized, water and air tolerant, green and often non-toxic.[4] The 2021 Nobel Prize in Chemistry award to Benjamin List and David W.C. MacMillan emboldens this assertion. In the past three decades, these multiple advantages have encouraged the rapid growth and acceptance of organocatalysis, but their application in electrocatalysis systems is rarely reported. This is probably because the performance of the specific

Q. Fan, J. Jiang, W. K. Pang, H. Liu, J. Wang, Z. Guo
Institute for Superconducting & Electronic Materials (ISEM)
Australian Institute of Innovative Materials (AIIM)
University of Wollongong
Wollongong, NSW 2522, Australia
E-mail: jiazhao@uow.edu.au; zaiping.guo@adelaide.edu.au

S. Zhang, Z. Guo
School of Chemical Engineering & Advanced Materials
The University of Adelaide
Adelaide, SA 5005, Australia

W. Lie
School of Chemistry and Molecular Bioscience
University of Wollongong
Wollongong, NSW 2500, Australia

Q. Gu
Australian Synchrotron
800 Blackburn Road, Clayton, VIC 3168, Australia

W. Yang
State Key Laboratory of Catalysis
Dalian Institute of Chemical Physics
Chinese Academy of Sciences
19A Yuquan Road, Dalian 116023, China

The ORCID identification number(s) for the author(s) of this article can be found under https://doi.org/10.1002/adfm.202212796

DOI: 10.1002/adfm.202212796

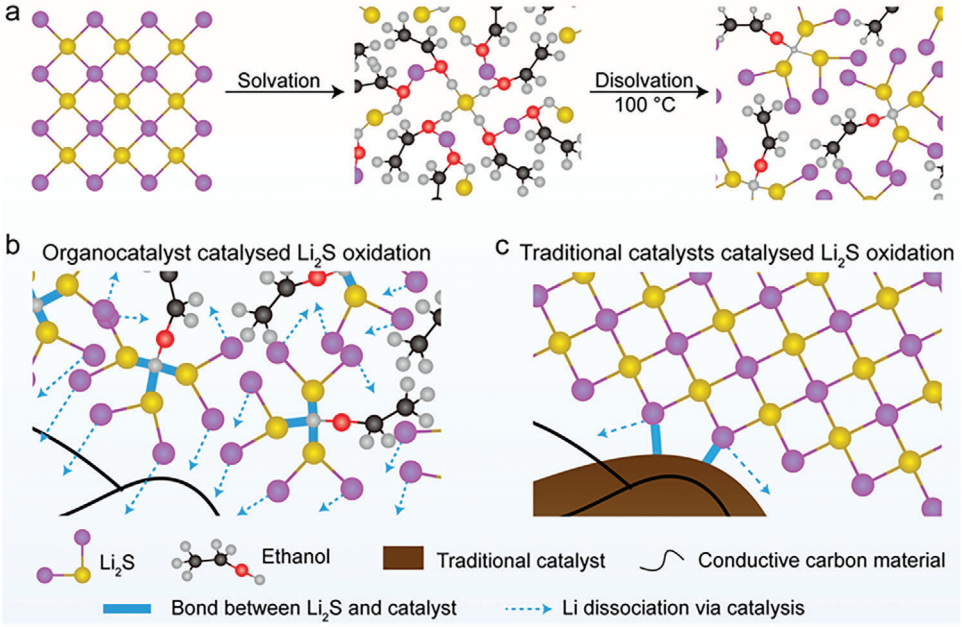

Figure 1. Two models for catalytic oxidation of Li_2S. a) Ethanol organocatalyst pre-bonded with Li_2S after solvation of Li_2S in an ethanol solvent and disolvation at 100 °C. The Li_2S is an ionic compound, so the individual Li^+ and S^{2-} ions dissociate and are solvated by the polar solvent (ethanol) and dispersed throughout the resulting solution, reducing the strong electrostatic forces between them.[8] b) A scheme showing that oxidation of Li_2S is catalyzed by the ethanol organocatalyst, which can pre-bond with Li_2S to form a uniform catalyst-Li_2S mixture. The ethanol organocatalyst functions effectively in Li_2S oxidation on a molecular scale, thus effectively promoting Li dissociation and accelerating oxidation of solid Li_2S, resulting in Li_2S cathodes with high capacity and reversibility. c) A scheme showing that oxidation of Li_2S is catalyzed by traditional solid catalysts. Because of limited solid-solid interfaces between the Li_2S and the traditional solid catalyst, most of the Li_2S could not contact the traditional solid catalyst surface and so becomes catalytically inactive, leading to inefficiency in Li dissociation, overall reaction kinetics, and the releasing capacity of Li_2S cathodes.

electrocatalytic process has a strong dependence on the organocatalysts selectivity. Although certain organic molecules have been leveraged to accelerate electrocatalysis,[5] they should be regarded as mediators or shuttles, acting as intermediate electron carriers or reservoirs without changing the transition state during reaction coordinate.[5b] Notably, the borders in terms of catalysts science for electrochemistry are no longer strictly set, and catalysts which are composed of nonmetal organic molecules can be characterized as organocatalyst. Nevertheless, no organocatalyst that exhibits high catalytic activity and selectivity has been developed for greener electrocatalysis to the best of our knowledge. Developing an effective organocatalyst to meet this demanding task is of great significance in organic and electrical chemistry.

As a proof of concept, we have recruited a commercially available ethanol solvent as a green and effective organocatalyst, to facilitate Li_2S oxidation in Li_2S cathodes for lithium–sulfur (sulphide) batteries. Such a battery must face the formidable challenge of extremely sluggish oxidation of Li_2S in the first charging process (overcoming the activation barrier) because of difficulty in Li^+ ions dissociation, restricting its potential to work as high-energy-density battery.[6] As shown in **Figure 1**, the pre-bonding between the ethanol organocatalyst and the Li_2S in material preparation (Figure 1a) can accurately catalyze the Li_2S oxidation on a molecular scale (Figure 1b), avoiding limited solid-solid catalytic interfaces in the traditional-solid-catalyzed system (Figure 1c), to effectively lower the charge potential and overcome the activation barrier of Li_2S cathodes. Based on the spectroscopy, crystallography, and theoretical calculations, we observed that when the ethanol molecules meet Li_2S particles, ethanol-bonded Li_2S composites form with strong S–H hydrogen bonds between the –OH groups of ethanol and the S^- of Li_2S, which was neglected in previous research of ethanol as an electrolyte additive.[7] The electrophilic H from the ethanol molecules is introduced into the Li_2S enabling the formation of strong S–H hydrogen bonds, and thus facilitating a change in the intrinsic electronic structure of Li_2S so as to rapidly dissociate Li ions during the catalytic cycle. Interestingly, a new mechanism of amorphized transformation from Li_2S to S in ethanol-bonded Li_2S cathodes has been revealed by operando technologies. By using ethanol organocatalyst, the activation barrier of Li_2S cathodes was overcome, decreasing the average charge voltage from 3.69 to 2.34 V, and contributing to increased specific capacity and cycling performance of Li_2S cathodes as well. This work presents an environmentally friendly, cost-efficient, and effective organocatalyst for Li_2S oxidation and provides important insights for the development of next-generation sustainable electrocatalysts.

2. Results and Discussion

2.1. Understanding the Interaction Between Li_2S and Ethanol

To uncover how ethanol interacts with Li_2S, first, we prepared and analyzed the structural variation within two Li_2S/ethanol solutions of different concentrations (0.55 M and saturated). ^1H Nuclear Magnetic Resonance (NMR) spectra in **Figure 2**a allow us to

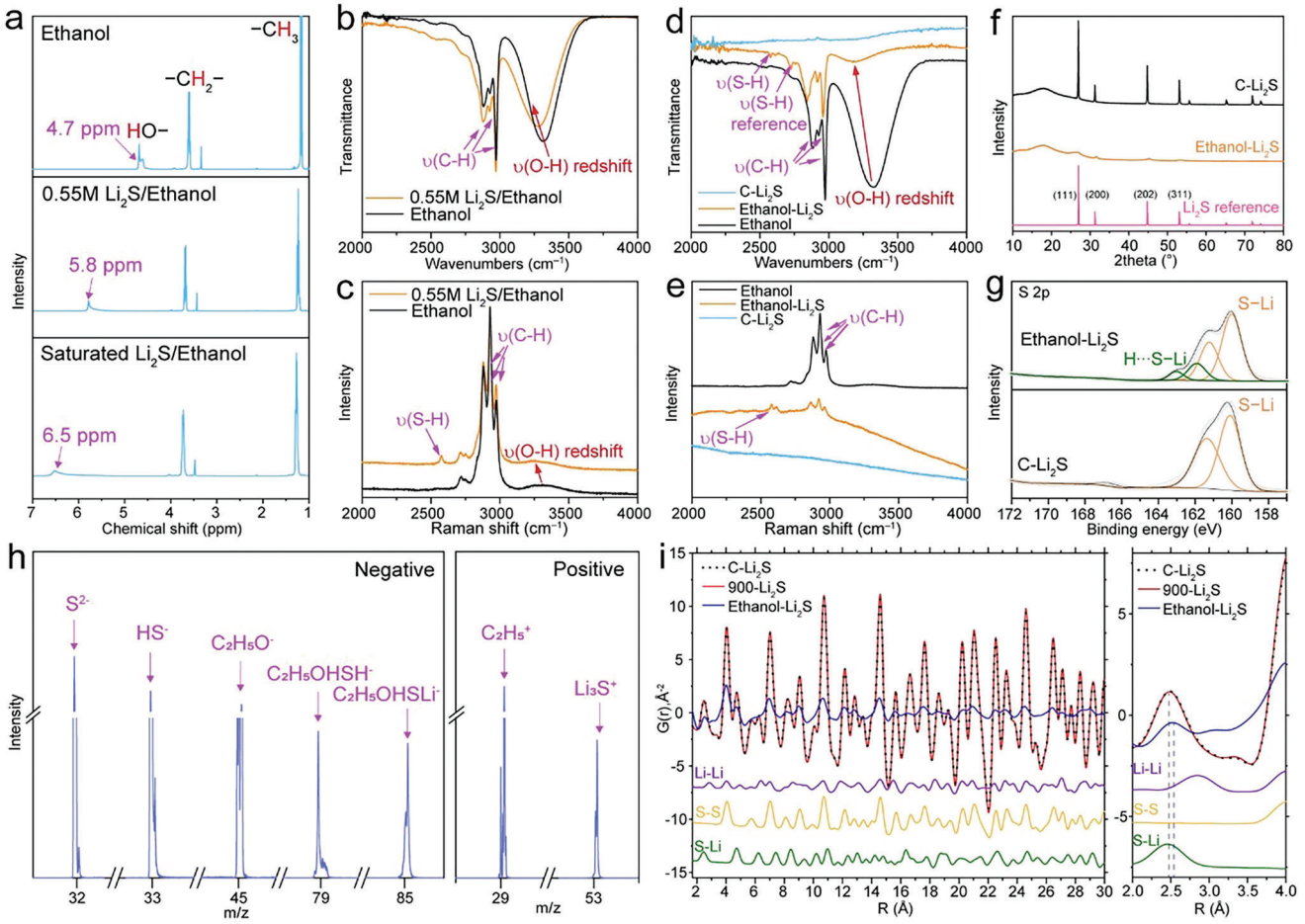

Figure 2. Interaction of Li_2S and ethanol. a) 1H NMR spectra of the ethanol, 0.55 M Li_2S/ethanol solution, and saturated Li_2S/ethanol solution. b) FTIR spectra of the ethanol and 0.55 M Li_2S/ethanol solution. c) Raman spectra of the ethanol and 0.55 M Li_2S/ethanol solutions. d) FTIR spectra of the ethanol, Ethanol−Li_2S, and commercial Li_2S (C−Li_2S) powder. e) Raman spectra of the ethanol, Ethanol−Li_2S powder, and C−Li_2S powder. f) XRD patterns of the Ethanol−Li_2S powder, C−Li_2S powder, and Li_2S reference (CollCode: 56 023). g) S 2p XPS spectra of the Ethanol−Li_2S powder and C−Li_2S powder. In the S 2p spectra, each pair of $2p_{3/2}$ and $2p_{1/2}$ spin-orbit doublets at lower and higher binding energy (BE), respectively, are shown by the same colour curves for each S chemical environment, and only the $2p_{3/2}$ peak will be described as conventional. h) Spectra of negative (left) and positive polarities (right) in the TOF-SIMS test of the Ethanol−Li_2S powder. i) Long-range (left) and short-range (right) PDF analysis of the Ethanol−Li_2S powder, 900−Li_2S, and C−Li_2S powder. The Li–Li, S–S, and S–Li curves were calculated from the Li_2S model (CollCode: 56 023) to show the standard distances of Li–Li, S–S, and S–Li for comparison.

assign the peaks at 3.6 and 1.2 ppm to the CH_2 and CH_3 groups of ethanol, respectively.[9] Clearly, the characteristic ^1H peak for the −OH groups moves significantly from 4.7 ppm in pure ethanol to 5.8 ppm and 6.5 ppm for the 0.55 M Li_2S/ethanol solution and the saturated Li_2S/ethanol solution, respectively, because the H is only from ethanol in the three solutions.[9] Apparently, the increasing broadness of the −OH with the Li_2S concentration is due to reduced molecular mobility, longer molecular tumbling time, and hence better and stronger contacts between −OH and Li_2S. Such results strongly indicate that the electronic structure of H in the −OH groups of ethanol molecules is dramatically influenced by Li_2S in Li_2S/ethanol solutions,[10] forming stronger intermolecular S···H−O hydrogen bonds between Li_2S and ethanol molecules due to the Lewis acidic (electrophilic) H in −OH and Lewis basic (nucleophilic) S in Li_2S.[11] Meanwhile, the ^7Li NMR (Figure S1, Supporting Information) also shows that a higher concentration of Li_2S in Li_2S/ethanol solutions leads to a downfield shift of Li in Li_2S, demonstrating a slight decrease in the electron density of Li owing to the S···H−O hydrogen bonds. For clear comparison, only pure ethanol and the 0.55 M Li_2S/ethanol solution were characterized by Fourier-Transform Infrared spectroscopy (FTIR) and Raman spectroscopy (Figure 2b,c). A redshift of the stretching vibration of O−H bonds was observed in pure ethanol and the 0.55 M Li_2S/ethanol solution, which indicates that stronger hydrogen bonds are formed between S and H in the Li_2S/ethanol solutions.[12] Notably, a stretching vibration of S−H bonds can be observed in the Raman spectrum of the 0.55 M Li_2S/ethanol solution (Figure 2c),[13] further supporting the proposition that ethanol (−OH group) can strongly bond with Li_2S (−S) through the formation of intermolecular S···H−O hydrogen bonds.

Employing ethanol solvent to dissolve the Li_2S, followed by evaporation of the ethanol, is a widespread approach to preparing the solid Li_2S cathode.[14] As demonstrated in Figure 2d,e,

however, both FTIR and Raman spectra of the Ethanol−Li_2S sample (dry powder of Li_2S/ethanol solution at 100 °C) show the characteristic vibration peaks of C–H and O–H bonds with ethanol molecules. It indicates the presence of ethanol molecules in the Ethanol−Li_2S solid powder, even though the powder was prepared at a temperature (100 °C) higher than the boiling point (78 °C) of ethanol solvents (Figure 2a–c). This is because S in Li_2S is more nucleophilic than O in ethanol,[15] resulting in a stronger hydrogen bond interaction between Li_2S and ethanol molecules than between ethanol and ethanol molecules. More importantly, a new stretching vibration attributed to S-H bonds can be observed in FTIR and Raman spectra of Ethanol−Li_2S (Figure 2d,e)[13] compared with the spectra of ethanol and commercial Li_2S (C−Li_2S), indicating a strong S···H–O chemical bond between the ethanol and the Li_2S in the dry Ethanol−Li_2S solid powder. It can be concluded that the S···H–O bonds formed between the Li_2S and ethanol molecules, and therefore, have much higher stability than the intrinsic O···H–O bonds among ethanol molecules, leaving the residual ethanol molecules in the Ethanol−Li_2S solid powder.

In Figure 2f, the laboratory X-ray diffraction (XRD) patterns of C−Li_2S show identical diffraction peaks to the Li_2S reference (CollCode: 56 023).[16] However, only small and broad peaks at the same diffraction angles of Li_2S in C−Li_2S are present in the pattern of the Ethanol−Li_2S sample, which indicates that the ethanol molecules can result in low crystallinity of Li_2S. In addition, similar alcohols and acetone were further used to verify our concept, but only methanol (apart from ethanol) can dissolve Li_2S (Figure S2a, Supporting Information). Methanol, moreover, is strongly reactive toward Li_2S due to highly electrophilic protons (H) in methanol, so a different crystalline structure is formed during drying of the Li_2S/methanol solution (Figure S2b, Supporting Information). The strongly electrophilic H, needed to form the intermolecular S···H–O hydrogen bonds with nucleophilic S, plays a critical role in dissolving Li_2S and leaving residual solvent molecules in the Li_2S structure after drying.

In addition, X-ray photoelectron spectroscopy (XPS) was employed to investigate the chemical environments of Li and S elements in both C−Li_2S and Ethanol−Li_2S (Figure 2g; Figure S3, Supporting Information). In the S 2p spectra, the S 2p spectrum of C−Li_2S demonstrates that the peaks located at 160.0 eV can be assigned to the S–Li bond, in accordance with the S 2p peaks of typical Li_2S.[17] Nevertheless, in the corresponding S 2p spectrum of the Ethanol−Li_2S, a new peak for S is located at 161.9 eV (1.9 eV higher than that for the S–Li bond), indicating a new chemical environment of S and the loss of electron density in S, which could be attributed to the influence of ethanol molecules and formation of O–H···S–Li hydrogen bonds (Figure 2,e). In addition to this, there is no apparent difference of Li 1s spectra for the Ethanol−Li_2S sample and the C−Li_2S sample (Figure S3, Supporting Information), demonstrating that the influence of the formation of hydrogen bonds on Li is negligible. Time-of-flight secondary-ion mass spectroscopy (TOS-SIMS) analysis in Figure 2h and Figure S4 (Supporting Informatuion) displays ion fragments of S^{2-}, HS^-, $C_2H_5O^-$, $C_2H_5OHSH^-$, and $C_2H_5OHSLi^-$ at mass-to-charge ratio (m/z) = 32, 33, 45, 79, and 85, respectively, in the spectra of negative polarities. Ion fragments of $C_2H_5^+$ and Li_3S^+ were also displayed at m/z = 29 and 53, respectively, in the spectra of positive polarities detected in the Ethanol−Li_2S sample. This result also demonstrates that the ethanol and Li_2S molecules can bind together via O–H···S–Li hydrogen bonds.

To further characterize the local atomic structure, pair distribution function (PDF) analysis was conducted, as shown in Figure 2i. Specifically, the PDF peaks in C−Li_2S show near superimposition of the calculated Li–Li, S–S, and S–Li curves from the Li_2S model, indicating the highly ordered and crystalline structure of Li_2S in the C−Li_2S sample. Nevertheless, the dampening of peaks in the Ethanol−Li_2S sample is clearly observed compared with what is observed in simulated Li-Li, S-S, and S-Li curves, indicating the presence of structural disorder in the Ethanol−Li_2S sample.[18] In the short-range (r ranging from 2.0 to 4.0 Å, Figure 2i), a longer S–Li distance can be observed in the curve for the Ethanol−Li_2S sample compared with the calculated S–Li bond (green line in Figure 2i), revealing a weaker bond and a decreased electron density between S and Li. To further confirm the result, the Ethanol−Li_2S sample was thermally treated at 900 °C under Ar flow to eliminate the ethanol molecules (900−Li_2S). The PDF curve of the obtained 900−Li_2S sample completely overlaps the curve of the C−Li_2S sample (Figure 2i), which shows a successful re-crystallization of Li_2S from its amorphous structure. It also shows that the hydrogen bonds between ethanol and Li_2S were destroyed by the high-temperature treatment. It should be noted that although the Ethanol−Li_2S is highly amorphous, the PDF data show a similar atomic arrangement to the highly crystalline Li_2S, based on the simulated pair distribution. According to the aforementioned structural characterization, it can surely be concluded that, in the Ethanol−Li_2S sample, ethanol (−OH groups, Lewis acid ions) can effectively bond with Li_2S (S, Lewis basic ions) via the formation of O–H···S–Li intermolecular hydrogen bonds, resulting in electron transfer from Li_2S to ethanol molecules. This fact indicates that the green and cheap ethanol potentially acts as an organocatalyst in electrochemical processes to accelerate redox reactions of Li_2S cathodes.

2.2. Electrochemical Performance of Ethanol-Catalyzed Li_2S Cathodes

To demonstrate that the ethanol can work as an organocatalyst to catalyze electrochemical oxidation of Li_2S, Ethanol−Li_2S/CNTs, 900−Li_2S/CNTs, and C−Li_2S/CNTs materials and electrodes were prepared from Ethanol−Li_2S powder, 900−Li_2S powder, and C−Li_2S powder, respectively. 900−Li_2S/CNTs electrodes were used to show the electrochemical performance after complete removal of the ethanol organocatalyst (based on the TGA-Ar and FTIR results in Figures S5 and S6, Supporting Information). The results of all electrochemical tests are shown in **Figure 3**. Notably, the galvanostatic charge and discharge curves at 0.1C (1C = 1167 mA g_{Li2S}^{-1}) in Figure 3a show that Ethanol−Li_2S/CNTs has a much lower average charge voltage (2.34 V at 600 mAh g^{-1}), which is ≈1.3 V lower than the average charge voltage for the 900−Li_2S/CNTs and C−Li_2S/CNTs (3.62 and 3.69 V respectively at 600 mAh g^{-1}). A small additional charging platform at ≈3.5 V at the end of charge process of the Ethanol−Li_2S/CNTs can be attributed to oxidation of a small amount of free Li_2S (ethanol-unbonded Li_2S), because oxidation of 900−Li_2S/CNTs and C−Li_2S/CNTs (pristine Li_2S) is

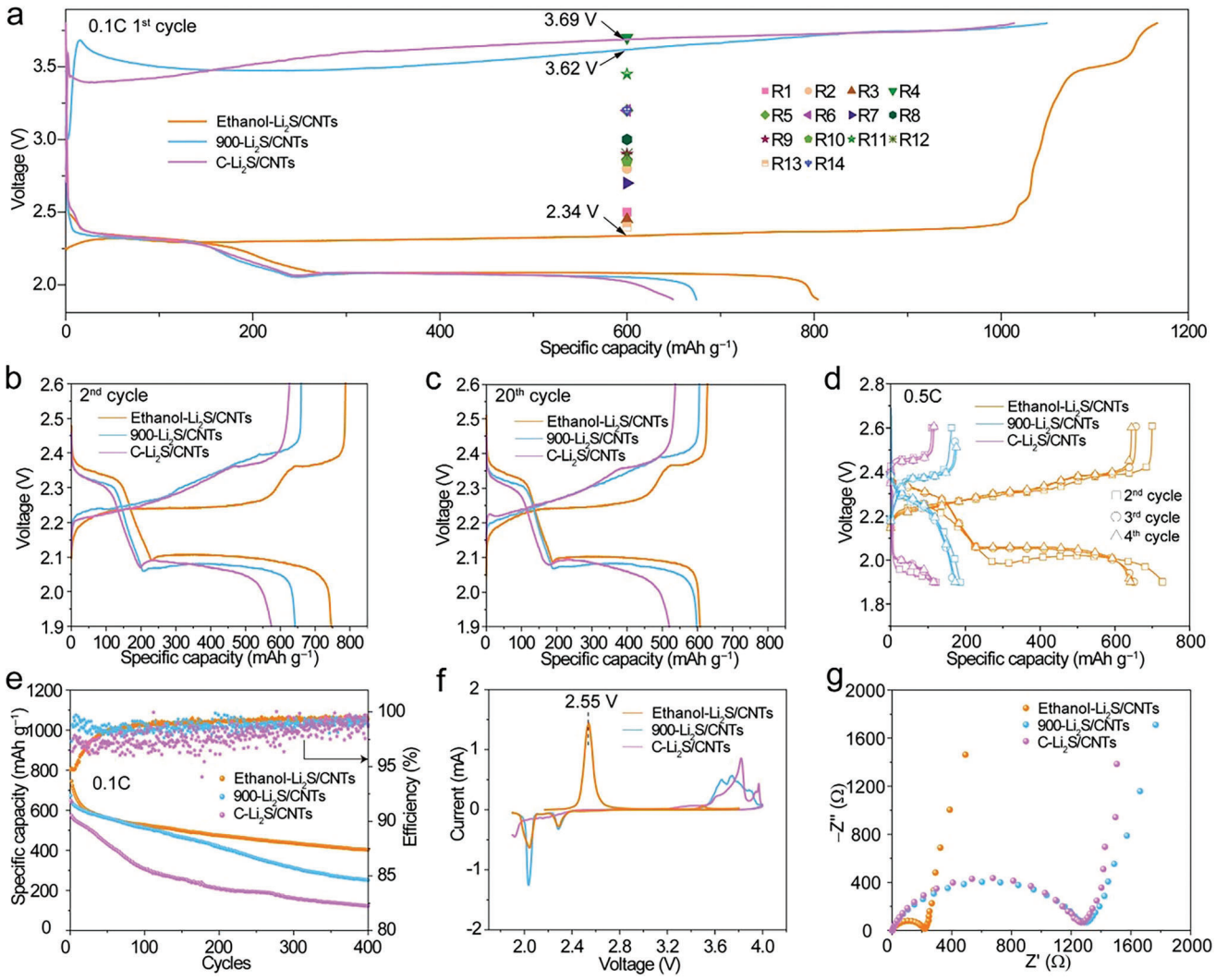

Figure 3. Electrochemical performance of ethanol-catalyzed Li_2S cathodes. Galvanostatic charge and discharge curves of the a) first, b) second, and c) 20th charge and discharge of the Ethanol−Li_2S/CNTs, 900−Li_2S/CNTs, and C−Li_2S/CNTs cathodes at 0.1C. R1,[14b] R2,[24] R3,[25] R4,[26] R5,[27] R6,[16a] R7,[14c] R8,[28] R9,[17b] R10,[17a] R11,[29] R12,[30] R13,[31] and R14[32] are mid-voltages of the reference reported cathodes in the first charge for comparison. d) Galvanostatic charge and discharge curves of the following three cycles at 0.5C after the first charge at 0.1C of the Ethanol−Li_2S/CNTs, 900−Li_2S/CNTs, and C−Li_2S/CNTs cathodes. e) Cycling performances of the Ethanol−Li_2S/CNTs, 900−Li_2S/CNTs, and C−Li_2S/CNTs cathodes at 0.1C. f) CV curves of the Ethanol−Li_2S/CNTs, 900−Li_2S/CNTs, and C−Li_2S/CNTs cathodes. g) EIS spectra of the fresh Ethanol−Li_2S/CNTs, 900−Li_2S/CNTs, and C−Li_2S/CNTs cathodes. 1C = 1167 mA g_{Li2S}^{-1}. The capacity calculation is based on the mass of Li_2S.

at ≈3.5 V. Except for two platforms at ≈2.3 (for ethanol-bonded Li_2S) and ≈3.5 V (for ethanol-unbonded Li_2S), there is no other platforms in the charge of Ethanol−Li_2S/CNTs, demonstrating that ethanol oxidation reactions (decomposition of ethanol) cannot occur in the range of the cut-off voltage. Galvanostatic intermittent titration technique (GITT) analysis in Figure S7 (Supporting Information) shows that the C−Li_2S/CNTs has a high overpotential of ≈1.0 V, but there is only ≈0.2 V overpotential in the Ethanol−Li_2S/CNTs. The results indicate that the ethanol organocatalyst can significantly accelerate the Li_2S oxidation and lower the activation barrier in the first charge process of Li_2S cathodes. Compared with previously reported Li_2S cathodes containing traditional solid electrocatalysts in references (Figure 3a), the Ethanol−Li_2S/CNTs cathode shows the lowest first charge overpotential, further confirming the great effectiveness of the green and cheap ethanol organocatalyst. By taking advantage of this characteristic, more Li_2S could be activated below the cut-off voltage and utilized to deliver a higher specific capacity in the Ethanol−Li_2S/CNTs than that in the 900−Li_2S/CNTs and C−Li_2S/CNTs.

In addition, in Figure S8a (Supporting Information), a peak is observed at the beginning of the first charge of the 900−Li_2S/CNTs and C−Li_2S/CNTs cathodes, demonstrating a larger activation barrier in the initial charge stage of the fresh Li_2S. This higher overpotential peak is attributed to contamination on the surface of Li_2S particles, or the worse reaction kinetics of initial Li ion dissociation.[19] The Ethanol−Li_2S/CNTs, however, show the absence of an activation barrier at the initial charge

stage of Li_2S (Figure S8a, Supporting Information) because of the catalytic effect of the ethanol organocatalyst. In Figure S8b (Supporting Information), higher voltage for Ethanol−Li_2S/CNTs than the 900−Li_2S/CNTs and C−Li_2S/CNTs at the second discharge plateau can be observed, which means a smaller overpotential for S reduction to Li_2S in the Ethanol−Li_2S/CNTs. The relative free energy data clearly show that the ethanol organocatalyst contributes more thermodynamically favorable discharging processes (Figure S9, Supporting Information). From the results, we can demonstrate that the green and cheap ethanol organocatalyst could not only accelerate Li_2S oxidation to S, but also promote S reduction to Li_2S, to achieve higher capacity in both charge and discharge processes.

Galvanostatic charge and discharge curves of the second and 20th cycles of the Ethanol−Li_2S/CNTs, 900−Li_2S/CNTs and C−Li_2S/CNTs are shown in Figure 3b,c, respectively, to demonstrate that the ethanol organocatalyst still funtioned well to accelerate the sulfur redox reactions after the first cycle. In the second and 20th cycles, like the first cycle, the Ethanol−Li_2S/CNTs containing ethanol organocatalyst shows the hugely different charge and discharge curves with the lowest overpotential, compared with the curves for the 900−Li_2S/CNTs and C−Li_2S/CNTs. The 900−Li_2S/CNTs and C−Li_2S/CNTs show the similar curves (especially charge curves), indicating the same uncatalyzed redox reaction mechanism in the 900−Li_2S/CNTs and C−Li_2S/CNTs. Notably, even lithium polysulphide (LiPS) transition mechanism is in the second and 20th cycles of 900−Li_2S/CNTs and C−Li_2S/CNTs,[16a,19b,20] the 900−Li_2S/CNTs, and C−Li_2S/CNTs still have higher overpotential than the Ethanol−Li_2S/CNTs in sulfur redox reactions, apparently demonstrating the ethanol organocatalyst is powerful and durable in catalyzing the sulfur redox reactions.

Moreover, the results for cells directly cycled at a current density of 0.5 C (after the 0.1 C charge to 3.8 V) are shown in Figure 3d. The 900−Li_2S/CNTs and C−Li_2S/CNTs exhibit larger overpotentials and less specific capacity than Ethanol−Li_2S/CNTs at the high current density, firmly supporting the fast S reduction kinetics in the Ethanol−Li_2S/CNTs. In addition, the inferior performance for C−Li_2S/CNTs at 0.5 C, compared with that for 900−Li_2S/CNTs at 0.5 C, is possibly attributable to the large particle size of Li_2S with the inhomogeneous mixture of commercial Li_2S and CNTs (Figure S10, Supporting Information). In Figure 3e, Ethanol−Li_2S/CNTs shows a lower coulombic efficiency and a quicker drop of specific capacity than 900−Li_2S/CNTs at the beginning of the cycling test, which should be attributed to unstable Li metal interface by a trace of dissolved ethanol in the Ethanol−Li_2S/CNTs cell (Figures S11–S13, Supporting Information). The ethanol can destroy the stable SEI causing severe polysulfide shuttle phenomenon, resulting in low coulombic efficiency at the initial cycling test.[21] After tens of cycles, the Li metal surface became more stable, and the Ethanol−Li_2S/CNTs cathode shows the best reversibility and superior coulombic efficiency, demonstrating high utilization of S species by the ethanol organocatalyst (Figure S13, Supporting Information). Although both 900−Li_2S/CNTs and C−Li_2S/CNTs have same highly crystalline Li_2S and no ethanol in the Li_2S structure (Figures S14 and S6, Supporting Information), the Li_2S particle size in C−Li_2S/CNTs is greatly larger than that in 900−Li_2S/CNTs (Figure S10, Supporting Information). Because of non-conductive nature of crystalline Li_2S, the Li_2S with larger particle size in C−Li_2S/CNTs can be hardly utilized, causing the dead Li_2S in the charge/discharge of the C−Li_2S/CNTs and thus less capacity and poor reversibility.

The cyclic voltammetry (CV) curves shown in Figure 3f show a distinct oxidation peak with a much lower voltage value of ≈2.55 V for the Ethanol−Li_2S/CNTs electrode, compared to those of the 900−Li_2S/CNTs (>3.6 V) and C−Li_2S/CNTs (>3.6 V). An incomplete reduction peak is obvious in the CV curve for C−Li_2S/CNTs, indicating the sluggish interfacial reactions from S to Li_2S due to larger Li_2S particles in C−Li_2S/CNTs (Figure S10, Supporting Information).[21b,22] Electrochemical impedance spectroscopy (EIS) was further conducted to show charge transfer resistance, as shown in Figure 3g. The smallest semicircle for the Ethanol−Li_2S/CNTs and the similar and huge semicircles for the fresh 900−Li_2S/CNTs and C−Li_2S/CNTs indicate that fast Li_2S oxidation reactions occurred in the Ethanol−Li_2S/CNTs cathodes, but the fresh 900−Li_2S/CNTs and C−Li_2S/CNTs show similar and sluggish kinetics in their faradic reactions.[23] To quantitatively evaluate the resistances, the R_e (the electrolyte resistance) and R_{ct} (the charge transfer resistance) are measured from the Nyquist plots (e.g., Figure S15, Supporting Information) and filled in the Table S1, Supporting Information. The charge transfer resistance of the Ethanol−Li_2S/CNTs (212.1 Ω) is an order of magnitude smaller than that in the 900−Li_2S/CNTs (1275 Ω) and C−Li_2S/CNTs (1242 Ω), indicating the fast redox reactions in the Ethanol−Li_2S/CNTs. The result of EIS is in accordance with the low activation barrier in the Ethanol−Li_2S/CNTs cathode and the similar high barrier in the 900−Li_2S/CNTs and C−Li_2S/CNTs cathodes (Figure 3a,b). Overall, the ethanol organocatalyst can accelerate the reaction kinetics of S reduction, and especially Li_2S oxidation with a low activation barrier in electrochemical reactions, resulting in a higher capacity and better reversibility in S based cathodes and achieving a greener and cheaper high-energy-density battery.

2.3. Synchrotron *Operando* and Ex situ Investigation into Ethanol-Catalyzed Li_2S Cathodes

To better investigate and understand the working mechanism of the ethanol organocatalyst in Li_2S cathodes during the cell operation, synchrotron *operando* X-ray diffraction (XRD) and synchrotron ex situ X-ray absorption spectroscopy (XAS) were conducted. According to the TGA results (Figure S5, Supporting Information), the 300−Li_2S/CNTs sample was elaborately synthesized by thermal treatment of the Ethanol−Li_2S/CNTs sample at 300 °C under Ar atmosphere to partially dissociate the ethanol, followed by an identical electrode preparation method to other Li_2S based electrodes. The collected synchrotron *operando* XRD results for Ethanol−Li_2S/CNTs, 300−Li_2S/CNTs, and 900−Li_2S/CNTs are shown in **Figure 4**a–c, respectively. At the beginning of charging, the representative (111) facet of Li_2S cannot be observed in Ethanol−Li_2S/CNTs samples because of the amorphous structure of Ethanol−Li_2S, which corresponds to the previous XRD and PDF results (Figure 2f,i; Figure S14, Supporting Information). A relatively higher crystallinity of the (111) lattice can be detected in the 300−Li_2S/CNTs because partial dissociation of ethanol at 300 °C results in the re-crystallization of

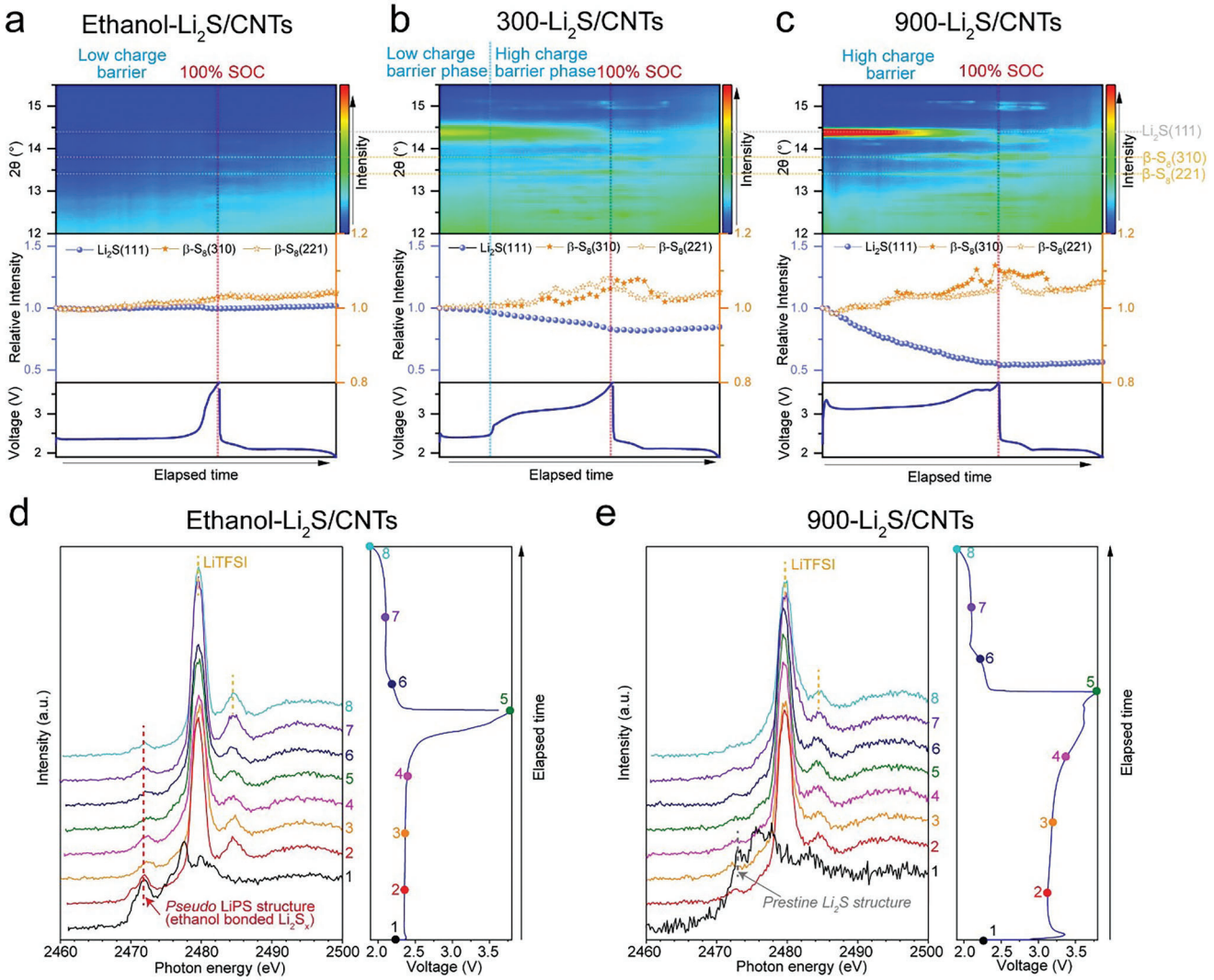

Figure 4. Characterization of ethanol-catalyzed Li_2S oxidation. The results of the synchrotron *operando* XRD experiments for the first cycle of the a) Ethanol−Li_2S/CNTs, b) 300−Li_2S/CNTs, and c) 900−Li_2S/CNTs cathodes. The contour plots on the top show the range of 12–15.5° from the XRD patterns. The colour bars on the right sides show the signal intensity, with the highest in red and the lowest in blue. The line plots of the change of intensity for the Li_2S (111), β-S_8(310), and β-S_8(221) peaks are shown in the middle. The corresponding galvanostatic charge and discharge curves are on the bottom to show the state of charge and depth of discharge. The results of the synchrotron ex situ soft XAS experiments on the (d) Ethanol−Li_2S/CNTs and (e) 900−Li_2S/CNTs cathodes. The sulfur K-edge XAS spectra are shown on the left. The corresponding galvanostatic charge and discharge curves are on the right to display the corresponding state of charge and depth of discharge. All cells were charged/discharged at the 0.1 C.

unbonded Li_2S species (Figures S5–S14, Supporting Information). A strong peak intensity attributed to the (111) facet can be found in the 900−Li_2S/CNTs sample, indicating highly crystalline Li_2S structure in the 900−Li_2S/CNTs sample (Figure 2i; Figure S14, Supporting Information).

Interestingly, no crystalline structure can be observed during charging and discharging the Ethanol−Li_2S/CNTs cathode, as evidenced by the relative peak intensity (Figure 4a). For the 900−Li_2S/CNTs cathode, however, the intensity of the Li_2S (111) lattice peak gradually decreased, along with the increased intensity of the β-S_8 (310) and β-S_8 (221) lattice peaks as the charging progressed (Figure 4c), demonstrating the progressive phase transition from crystalline Li_2S to crystalline β-S_8 without the formation of soluble LiPSs.[20,33] Clearly, charging the 300−Li_2S/CNTs cathode at the initial charging stage (also the low charge barrier phase) results in no change in the intensities at the 2θ positions for the Li_2S (111), β-S_8 (310), and β-S_8 (221) (Figure 4b), resembling the charging process for the Ethanol−Li_2S/CNTs cathode (Figure 4a). However, the intensities rapidly change at the following charge stage (also the high charge barrier phase) (Figure 4b), which is consistent with the charge of the 900−Li_2S/CNTs (Figure 4c). Like the Li_2S (111), the Li_2S (200) also confirmed the different oxidation behaviours of the Li_2S (Figure S16, Supporting Information). The *operando* XRD results for the 300−Li_2S/CNTs sample, therefore, indicate that the low activation barrier is highly related to the charge of

non-crystalline Li_2S, while the high activation barrier is attributable to the charge of crystalline Li_2S. Because some ethanol molecules still existed in the 300−Li_2S/CNTs (Figures S5, S6, Supporting Information), a certain amount of Li_2S bonded with the ethanol would exhibit an amorphous structure of Li_2S, which will initially be oxidised in the activation process, contributing to the low charge barrier phase compared to that in 900−Li_2S/CNTs. Free Li_2S with high crystallinity, however, can only be oxidised at a high potential to overcome the high activation barrier. In addition, the (111) facet in 900−Li_2S/CNTs can be observed even after the first charge process (Figure 4c), which means that not all the Li_2S material was fully activated, explaining the lower specific capacity in 900−Li_2S/CNTs (Figure 3a). All the synchrotron *operando* XRD results indicate that the ethanol organocatalyst can induce the transition from amorphous Li_2S to amorphous S, lowering the charge voltage during redox reactions.

Synchrotron ex situ soft XAS was employed to collect more information on the operation of the Li_2S cathodes. The sulfur *K*-edge XAS spectrum of Ethanol−Li_2S suggest the *pseudo* LiPS structure in Ethanol−Li_2S (Figure S17, Supporting Information). Moreover, Figure 4d shows the featured *pseudo* LiPS absorption peak of ethanol-bonded S species throughout the whole charge and discharge process of Ethanol−Li_2S/CNTs. This result demonstrates that the ethanol can bond with S species and work as an electrocatalyst during the operation of S-based cathodes, leading to the *pseudo* LiPS transition mechanism for Li_2S oxidation. The soft XAS results show that the characteristic peaks of pure Li_2S disappear at the beginning of charging 900−Li_2S/CNTs (Figure 4e). It seems that the soft XAS results contradict the results of the synchrotron *operando* XRD for the 900−Li_2S/CNTs cathode (indicating that crystalline Li_2S is presented in the whole charge process) (Figure 4c), but this contradiction exists because the synchrotron *operando* XRD can characterize the bulk structure of Li_2S particles, while synchrotron ex situ soft XAS can only provide information from the surfaces of Li_2S particles. The surfaces of the Li_2S particles were immediately covered with crystalline S at the start of charging the 900−Li_2S/CNTs cathode,[20] leading to difficulty in detection of the crystalline Li_2S by soft XAS. Moreover, the formed S cannot be observed in the sulfur ex situ XAS K-edge spectra, possibly due to overlapping with the strong signals of the Lithium bis(trifluoromethanesulfonyl)imide (LiTFSI) salt from the electrolyte.

A schematic illustration of the mechanism behind the Li_2S and Ethanol−Li_2S oxidation process is depicted in Figure S18 (Supporting Information). The oxidation of pure Li_2S requires a high charge overpotential and results in the direct formation of crystalline S from crystalline Li_2S on the unreacted Li_2S surface. In this case, the oxidation of the remaining Li_2S core with the thicker and highly non-conductive crystalline S shell becomes harder, causing continuous increase of charge voltage, the loss of active materials and thus, lower capacity in the Li_2S cathode. In the case of the oxidation of ethanol bonded Li_2S, the ethanol organocatalyst can lead to the transition from amorphous Li_2S to amorphous S. During the reactions, the bonded Li_2S species can be rapidly oxidized with the help of the ethanol organocatalyst to overcome the activation barrier and fully utilize the Li_2S, releasing more capacity.

2.4. Theoretical Understanding of Ethanol-Catalyzed Li_2S Cathodes

Because the ethanol could dissociate the long-range structure of Li_2S (Figure S19, Supporting Information), further theoretical calculations were based on the Li_2S molecule and the ethanol molecule to clearly demonstrate the influence of ethanol on $Li_2S_{(x)}$ electronic structure and dissociation behavior. The binding energies (**Figure 5**a), electrostatic potential (ESP) distribution (Figure 5b), and Li dissociation reaction free energy (Figure 5c) of ethanol bonded S species were analyzed by Density Functional Theory (DFT) calculations. The binding energies between the ethanol molecule and the respective Li_2S, Li_2S_2, Li_2S_4, Li_2S_6, Li_2S_8, and S_8 molecules are −2.45, −1.85, −1.42, −1.28, −1.27, and −0.23 eV, respectively (Figure 5a). For the optimised structure of Ethanol−Li_2S, Ethanol−Li_2S_2, and Ethanol−Li_2S_4, the H atoms in -OH groups of ethanol molecules strongly bond with S atoms in the short-chain LiPSs as shown in Figure 5a because the strongly nucleophilic S in the short-chain LiPSs can interact with electrophilic H in the −OH group, supported by the shorter distance of S and H in those three structures (Table S2, Supporting Information). The highest binding energies, therefore, could be achieved between ethanol and short-chain LiPSs (Li_2S, Li_2S_2, and Li_2S_4). For the electronic structure of Ethanol−Li_2S_6 and Ethanol−Li_2S_8, the S atoms are more electroneutral due to less concentration of Li atoms in the molecular structures, which leads to a weaker interaction and longer distance between S and H (Table S2, Supporting Information). The interaction and distance between O in the −OH group and Li in the long-chain LiPSs (Li_2S_6 and Li_2S_8) contribute more to binding energies of Ethanol−Li_2S_6 and Ethanol−Li_2S_8. The smallest binding energy of Ethanol−S_8 is because the ethanol can hardly bond with the totally electroneutral S_8.

Electrostatic potential (ESP) contour mapping was conducted from DFT calculations, as shown in Figure 5b. From the ESP contour mapping, it can be observed that the S atom in Li_2S is highly nucleophilic and the H atom in −OH is highly electrophilic, promoting bonding between the S atom in Li_2S and H atom in −OH of ethanol. Furthermore, the ESP of the S atom in CH_3CH_2OH−Li_2S becomes more positive (compared with the S atom in the Li_2S molecule), indicating that the ethanol molecule withdraws electron density from S, consistent with the results of XPS (Figure 2g). The lower electron density of S in the Ethanol−Li_2S means weaker S–Li bonds (consistent with the longer S–Li bonds in the PDF analysis in Figure 2i) that make the breakage of S–Li bonds more thermodynamically favorable and allow fast Li_2S oxidation.

Figure 5c shows that the reaction free energies for the Li dissociation process in pristine Li_2S are 1.88 eV, while only 1.13 eV is sufficient for dissociating Li from the Ethanol−Li_2S complex. The lower reaction free energy for Ethanol−Li_2S should be attributed to the loss of electron density in the S atom (Figure 2g,b), decreasing the strength of the Li–S bond and making the dissociation of Li ions more kinetically favorable. The results demonstrate that the green and cheap ethanol organocatalyst can efficiently accelerate the Li_2S oxidation on a molecular scale, and can overcome the activation barrier in the first charge of Li_2S cathodes to allow the S-based batteries to have a high-energy-density, and be more cost-efficient, and environmentally friendly.

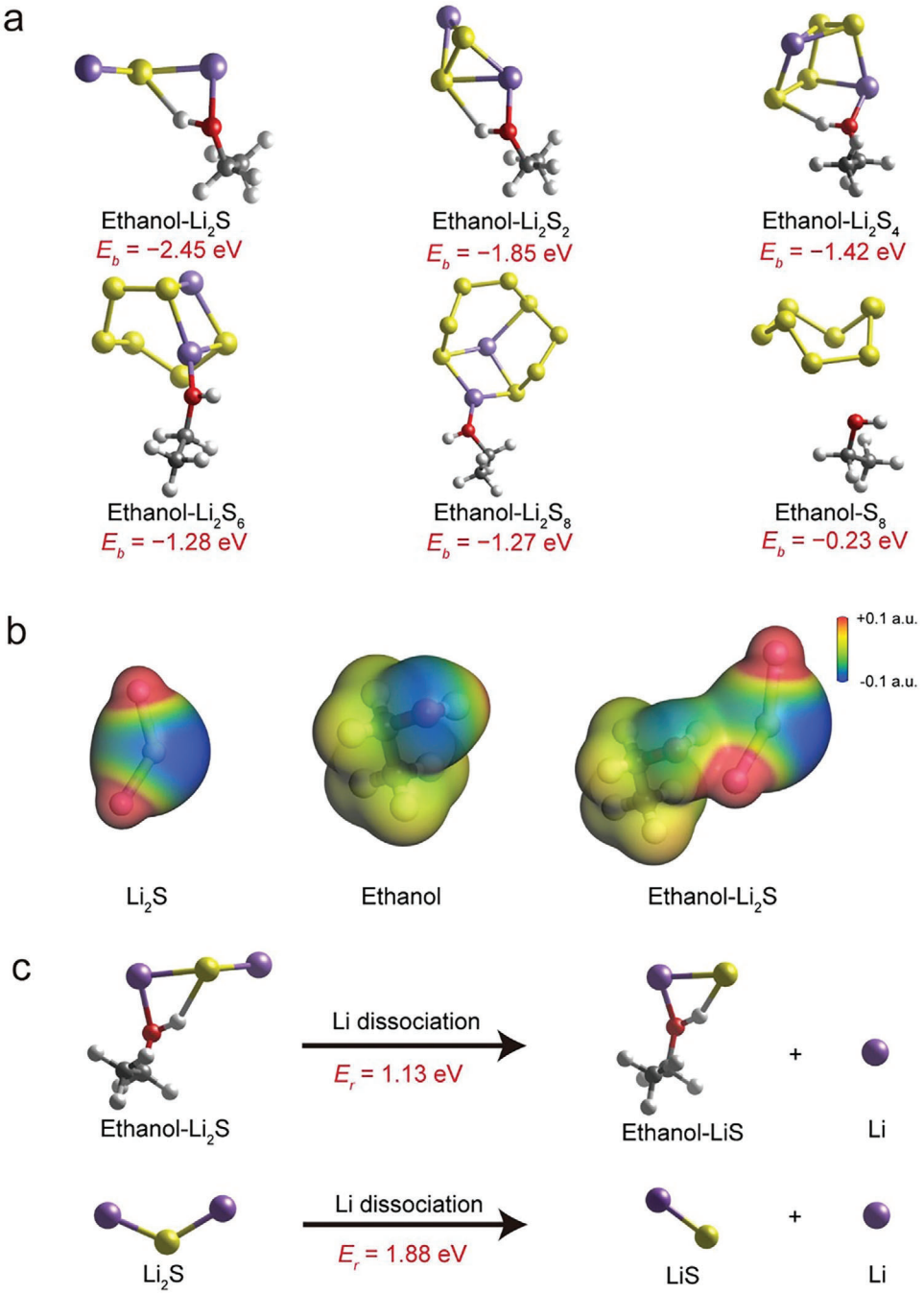

Figure 5. Theoretically understanding reaction mechanism of ethanol-catalyzed Li_2S oxidation. (a) Optimised geometric structures and binding energies of ethanol bonded Li_2S, Li_2S_2, Li_2S_4, Li_2S_6, Li_2S_8, and S_8 from DFT calculations. E_b is the binding energy between ethanol and corresponding S species. b) Electrostatic potential distributions for the Li_2S (left), ethanol (middle), and ethanol bonded Li_2S (right) molecules obtained by DFT calculations. Regions with a negative electrostatic potential (ESP) (blue) have a higher tendency for nucleophilic reactions, while electrophilic reactions are more favorable in regions of more positive ESP (red). (c) The reaction free energies and optimised structures from DFT calculations of the dissociation of Li ions in the Li_2S and Ethanol—Li_2S. The yellow, purple, red, grey, and white balls denote the S, Li, O, C, and H atoms, respectively. E_r is the reaction free energy for Li dissociation.

3. Conclusion

In this study, the ethanol organocatalyst was introduced into the Li_2S structure to form Ethanol–Li_2S composites as Li_2S cathode materials. The ethanol organocatalyst can accelerate the reaction kinetics of S reduction and Li_2S oxidation on a molecular scale. With the ethanol organocatalyst, the activation barrier of Li_2S cathodes was overcome and the first charge voltage plateau was lowered from 3.69 to 2.34 V, with higher specific capacity and better cycling performance obtained simultaneously. The theoretical and experimental results indicate that the ethanol molecules can bond with Li_2S through the formation of O–H···S intermolecular hydrogen bonds, enabling the loss of electron density in the S element and thus promoting fast dissociation of Li ions during the charging process. Synchrotron *operando* and ex situ techniques revealed a unique *pseudo* LiPS transition mechanism in the oxidation of the ethanol bonded Li_2S. This environmentally friendly, cost-efficient, and more effective ethanol organocatalyst exhibits high potential for cheaper and greener S-based electrodes in high-energy-density Li–S and S-based Li-ion batteries. For the further practical research, the high loading electrode and lean electrolyte need to be considered with the organocatalysts, and the influence of the organocatalysts on the anode should also be investigated. This work may guide the development of a new series of sustainable electrocatalysts from organocatalysts to meet the challenges in electrochemistry.

Supporting Information

Supporting Information is available from the Wiley Online Library or from the author.

Acknowledgements

Q.F. and S.Z. contributed equally to this work. The authors gratefully appreciate the financial support provided by the Australian Research Council (ARC) (Nos. LP160100914, DP180101453, and FL210100050). The authors thank the UOW Electron Microscopy Centre for equipment use, the Australian Synchrotron (ANSTO) (Nos. AS192/PD/14632 and AS212/SXR/17250) for the tests in the Powder Diffraction (PD) and soft X-ray Adsorption Spectroscopy (Soft XAS) beamlines, and surface analysis laboratory, SSEAU, MWAC, UNSW for TOF-SIMS analysis as well. Many thanks also go to Dr. Tania Silver for her critical reading of the manuscript and Dr. Zhijie Wang and Ms. Yanyan Wang for their suggestions and comments.

Open access publishing facilitated by University of Wollongong, as part of the Wiley - University of Wollongong agreement via the Council of Australian University Librarians.

Conflict of Interest

The authors declare no conflict of interest.

Data Availability Statement

The data that support the findings of this study are available from the corresponding author upon reasonable request.

Keywords

electrochemical oxidation, ethanol, hydrogen bonds, Li_2S cathode, Li–S batteries, organocatalysts

Received: November 29, 2022
Revised: January 15, 2023
Published online: May 14, 2023

[1] a) T. Y. Ma, S. Dai, S. Z. Qiao, *Mater. Today* **2016**, *19*, 265; b) C. Wei, S. Sun, D. Mandler, X. Wang, S. Z. Qiao, Z. J. Xu, *Chem. Soc. Rev.* **2019**, *48*, 2518.
[2] a) I. L. C. Buurmans, B. M. Weckhuysen, *Nat. Chem.* **2012**, *4*, 873; b) H. Jin, C. Guo, X. Liu, J. Liu, A. Vasileff, Y. Jiao, Y. Zheng, S.-Z. Qiao, *Chem. Rev.* **2018**, *118*, 6337.
[3] A. Studer, D. P. Curran, *Nat. Chem.* **2014**, *6*, 765.
[4] a) M. P. van der Helm, B. Klemm, R. Eelkema, *Nat. Rev. Chem.* **2019**, *3*, 491; b) D. W. C. Macmillan, *Nature* **2008**, *455*, 304.
[5] a) A. G. Tamirat, X. Guan, J. Liu, J. Luo, Y. Xia, *Chem. Soc. Rev.* **2020**, *49*, 7454; b) Z.-W. Zhang, H.-J. Peng, M. Zhao, J.-Q. Huang, *Adv. Funct. Mater.* **2018**, *28*, 1707536; c) Y. Tsao, M. Lee, E. C. Miller, G. Gao, J. Park, S. Chen, T. Katsumata, H. Tran, L.-W. Wang, M. F. Toney, Y. Cui, Z. Bao, *Joule* **2019**, *3*, 872.
[6] a) D. Su, D. Zhou, C. Wang, G. Wang, *Adv. Funct. Mater.* **2018**, *28*, 1800154; b) J. Jiang, Q. Fan, S. Chou, Z. Guo, K. Konstantinov, H. Liu, J. Wang, *Small* **2021**, *17*, 1903934; c) S. Li, D. Leng, W. Li, L. Qie, Z. Dong, Z. Cheng, Z. Fan, *Energy Stor. Mater.* **2020**, *27*, 279; d) Y. Son, J.-S. Lee, Y. Son, J.-H. Jang, J. Cho, *Adv. Energy Mater.* **2015**, *5*, 1500110; e) X. Meng, Y. Liu, L. Yu, J. Qiu, Z. Wang, *Adv. Funct. Mater.* **2022**, *33*, 2211062, ; f) L. K. J. Ting, Y. Gao, H. Wang, T. Wang, J. Sun, J. Wang, *ACS Omega* **2022**, *7*, 40682; g) X. Zhang, H. Yang, Y. Sun, Y. Yang, *ACS Appl. Mater. Interfaces* **2022**, *14*, 41003; h) X. Qi, F. Yang, P. Sang, Z. Zhu, X. Jin, Y. Pan, J. Ji, R. Jiang, H. Du, Y. Ji, Y. Fu, L. Qie, Y. Huang, *Angew. Chem., Int. Ed.* **2023**, *62*, e202218803.
[7] X. Liang, J. Yun, K. Xu, P. Shi, Y. Sun, C. Chen, H. Xiang, *Chem. Commun.* **2019**, *55*, 10088.
[8] T. L. Brown, *Chemistry: the central science*, 11th ed., Pearson Education, NJ **2009**.
[9] a) E. D. Becker, U. Liddel, J. N. Shoolery, *J. Mol. Spectrosc.* **1958**, *2*, 1; b) I. P. Gerothanassis, A. Troganis, V. Exarchou, K. Barbarossou, *Chem. Educ. Res. Pract.* **2002**, *3*, 229.
[10] F. M. A. Wendt, J. Meiler, F. Weinhold, T. C. Farrar, *Mol. Phys.* **1998**, *93*, 145.
[11] a) Z. Wang, Y. Wang, Z. Zhang, X. Chen, W. Lie, Y.-B. He, Z. Zhou, G. Xia, Z. Guo, *Adv. Funct. Mater.* **2020**, *30*, 2002414; b) F. Yang, J. Hao, J. Long, S. Liu, T. Zheng, W. Lie, J. Chen, Z. Guo, *Adv. Energy Mater.* **2021**, *11*, 2003346.
[12] T. Fornaro, D. Burini, M. Biczysko, V. Barone, *J. Phys. Chem. A* **2015**, *119*, 4224.
[13] a) G. E. McManis, L. E. Gast, *J. Am. Oil Chem. Soc.* **1974**, *51*, 198; b) H. Li, C. J. Wurrey, G. J. Thomas, *J. Am. Chem. Soc.* **1992**, *114*, 7463; c) J. Y. Horiba, Raman data and analysis: Raman spectroscopy for analysis and monitoring, http://horiba.com/fileadmin/uploads/Scientific/Documents/Raman/bands.pdf (accessed: January, 2022); d) M.-È. Gosselin, C. J. Kapustij, U. D. Venkateswaran, V. R. Leverenz, F. J. Giblin, *Exp. Eye Res.* **2007**, *84*, 493.
[14] a) D.-H. Wang, D. Xie, X.-H. Xia, X.-Q. Zhang, W.-J. Tang, Y. Zhong, J.-B. Wu, X.-L. Wang, J.-P. Tu, *J. Mater. Chem. A* **2017**, *5*, 19358; b) J. He, Y. Chen, A. Manthiram, *Adv. Energy Mater.* **2019**, *9*, 1900584; c) J. Jiang, Q. Fan, Z. Zheng, M. R. Kaiser, Q. Gu, S. Chou, K. Konstantinov, J. Wang, *ACS Appl. Energy Mater.* **2020**, *3*, 6447.
[15] a) C. K. Ingold, *Chem. Rev.* **1934**, *15*, 225; b) F. A. Carey, R. J. Sundberg, *Advanced Organic Chemistry: Part A: Structure and Mechanisms*, 5th ed., Springer, NY **2007**.
[16] a) Q. Fan, J. Jiang, S. Zhang, T. Zhou, W. K. Pang, Q. Gu, H. Liu, Z. Guo, J. Wang, *Adv. Energy Mater.* **2021**, *11*, 2100957; b) T. Seita, Y.

Matsumae, J. L. Liu, R. Tatara, K. Ueno, K. Dokko, M. Watanabe, *ACS Energy Lett.* **2020**, *5*, 1.

[17] a) M. L. Yu, Z. Y. Wang, Y. W. Wang, Y. F. Dong, J. S. Qiu, *Adv. Energy Mater.* **2017**, *7*, 1700018; b) J. Zhang, Y. Shi, Y. Ding, L. Peng, W. Zhang, G. Yu, *Adv. Energy Mater.* **2017**, *7*, 1602876.

[18] J. M. Stratford, A. K. Kleppe, D. S. Keeble, P. A. Chater, S. S. Meysami, C. J. Wright, J. Barker, M.-M. Titirici, P. K. Allan, C. P. Grey, *J. Am. Chem. Soc.* **2021**, *143*, 14274.

[19] a) Y. Jung, B. Kang, *Phys. Chem. Chem. Phys.* **2016**, *18*, 21500; b) Y. Yang, G. Zheng, S. Misra, J. Nelson, M. F. Toney, Y. Cui, *J. Am. Chem. Soc.* **2012**, *134*, 15387.

[20] L. Zhang, D. Sun, J. Feng, E. J. Cairns, J. Guo, *Nano Lett.* **2017**, *17*, 5084.

[21] a) Y. V. Mikhaylik, J. R. Akridge, *J. Electrochem. Soc.* **2004**, *151*, A1969; b) G. Li, S. Wang, Y. Zhang, M. Li, Z. Chen, J. Lu, *Adv. Mater.* **2018**, *30*, 1705590.

[22] a) L. Kong, J.-X. Chen, H.-J. Peng, J.-Q. Huang, W. Zhu, Q. Jin, B.-Q. Li, X.-T. Zhang, Q. Zhang, *Energy Environ. Sci.* **2019**, *12*, 2976; b) S. Drvarič Talian, G. Kapun, J. Moškon, A. Vizintin, A. Randon-Vitanova, R. Dominko, M. Gaberšček, *Chem. Mater.* **2019**, *31*, 9012; c) S. S. Zhang, *Energies* **2012**, *5*, 5190.

[23] a) S. S. Zhang, K. Xu, T. R. Jow, *J. Power Sources* **2003**, *115*, 137; b) S. S. Zhang, K. Xu, T. R. Jow, *Electrochim. Acta* **2004**, *49*, 1057.

[24] G. Tan, R. Xu, Z. Xing, Y. Yuan, J. Lu, J. Wen, C. Liu, L. Ma, C. Zhan, Q. Liu, T. Wu, Z. Jian, R. Shahbazian-Yassar, Y. Ren, D. J. Miller, L. A. Curtiss, X. Ji, K. Amine, *Nat. Energy* **2017**, *2*, 17090.

[25] J. Wang, L. Jia, S. Duan, H. Liu, Q. Xiao, T. Li, H. Fan, K. Feng, J. Yang, Q. Wang, M. Liu, J. Zhong, W. Duan, H. Lin, Y. Zhang, *Energy Stor. Mater.* **2020**, *28*, 375.

[26] S.-H. Chung, P. Han, C.-H. Chang, A. Manthiram, *Adv. Energy Mater.* **2017**, *7*, 1700537.

[27] Y. Peng, Y. Zhang, Z. Wen, Y. Wang, Z. Chen, B.-J. Hwang, J. Zhao, *Chem. Eng. J.* **2018**, *346*, 57.

[28] F. Ye, H. Noh, J. Lee, H. Lee, H.-T. Kim, *J. Mater. Chem. A* **2018**, *6*, 6617.

[29] Y. Chen, S. Lu, J. Zhou, X. Wu, W. Qin, O. Ogoke, G. Wu, *J. Mater. Chem. A* **2017**, *5*, 102.

[30] Z. Jiao, L. Chen, J. Si, C. Xu, Y. Jiang, Y. Zhu, Y. Yang, B. Zhao, *J. Power Sources* **2017**, *353*, 167.

[31] Z. Wang, C. Xu, L. Chen, J. Si, W. Li, S. Huang, Y. Jiang, Z. Chen, B. Zhao, *Electrochim. Acta* **2019**, *312*, 282.

[32] L. Xue, L. Zeng, W. Kang, H. Chen, Y. Hu, Y. Li, W. Chen, T. Lei, Y. Yan, C. Yang, A. Hu, X. Wang, J. Xiong, C. Zhang, *Adv. Energy Mater.* **2021**, *11*, 2100420.

[33] A. Vizintin, L. Chabanne, E. Tchernychova, I. Arcon, L. Stievano, G. Aquilanti, M. Antonietti, T. P. Fellinger, R. Dominko, *J. Power Sources* **2017**, *344*, 208.